The Astrophysical Journal, 668:993–1000, 2007 October 20

CARBONATES IN SPACE: THE CHALLENGE OF LOW-TEMPERATURE DATA[1]

Th. Posch and A. Baier
Institut für Astronomie, Türkenschanzstraße 17, A-1180 Vienna, Austria; posch@astro.univie.ac.at

H. Mutschke
Astrophysikalisches Institut, Schillergässchen 2-3, D-07745 Jena, Germany

and

Th. Henning
Max-Planck-Institut für Astronomie (MPIA), Königstuhl 17, D-69117 Heidelberg, Germany
Received 2007 May 4; accepted 2007 July 7

ABSTRACT

Carbonates have repeatedly been discussed as possible carriers of stardust emission bands. However, the band assignments proposed so far were mainly based on room-temperature powder transmission spectra of the respective minerals. Since very cold calcite grains have been claimed to be present in protostars and in planetary nebulae (PNs) such as NGC 6302, the changes of their dielectric functions at low temperatures are relevant from an astronomical point of view. We have derived the infrared optical constants of calcite and dolomite from reflectance spectra, measured at 300, 200, 100, and 10 K, and calculated small-particle spectra for different grain shapes, with the following results. (1) The absorption efficiency factors of both calcite and dolomite are extremely dependent on the particle shapes. This is due to the high peak values of the optical constants of $CaCO_3$ and $CaMg[CO_3]_2$. (2) The far-infrared properties of calcite and dolomite also depend very significantly on the temperature. Below 200 K, a pronounced sharpening and increase in the band strengths of the far-infrared resonances occurs. (3) In view of the intrinsic strength and sharpening of the $\sim$44 μm band of calcite at 200–100 K, the absence of this band, inferred from *Infrared Space Observatory* data, in PNs requires dust temperatures below 45 K. (4) Calcite grains at such low temperatures can account for the "92" μm band, while our data rule out dolomite as the carrier of the 60–65 μm band. The optical constants presented here are publicly available in the AIU Jena Database of Optical Constants for Cosmic Dust.

Subject headings: circumstellar matter — infrared: stars — methods: laboratory — stars: AGB and post-AGB — stars: atmospheres

1. INTRODUCTION

In the 1970s carbonates were proposed as carriers of mid-infrared features detected in astronomical spectra, such as the 11.3 μm emission band seen in NGC 7027 and in the "Red Rectangle" (Gillet et al. 1973; Bregman & Rank 1975; Bregman 1977).

In parallel to that, reflectance spectra of calcite ($CaCO_3$) and magnesite ($MgCO_3$) have been measured in the laboratory. Hellwege et al. (1970) did the measurements in the whole mid- and far-infrared range for calcite, magnesite, and dolomite ($CaMg[CO_3]_2$), while Penman (1976) examined calcite and magnesite in the 5–50 μm region. All these measurements have been carried out at room temperature.

Carbonate grains have been found in interplanetary dust particles (IDPs). Sandford (1986) and Tomeoka & Buseck (1986) reported the identification of carbonate minerals in IDPs both by a chemical dissolution experiment and by transmission electron microscopy. As shown by Tomeoka & Buseck (1986), the mineralogy of the IDP carbonates is essentially that of breunnerite, an Mg-rich solid solution of magnesite and siderite ($FeCO_3$). Solid solutions of Ca- and Mg-carbonates are rare in the IDPs examined so far (see also Joswiak & Brownlee 2001). It is of note that the IDPs show a 6.8 μm absorption feature which is probably due to the stretching vibration of carbonate anions (Sandford 1986). It must be noted, however, that there are doubts on this identification, because the carbonate band at 11.4 μm was not detected in a study of five IDPs (Quirico et al. 2000). A band similar to the 6.8 μm feature is supposedly seen in the spectra of the *Deep Impact* ejecta from comet 9P/Tempel 1 measured with the *Spitzer* IRS spectrometer (Lisse et al. 2006). In these spectra, bands at 11–12 and 13–14 μm have also been assigned to carbonates.

While the identification of the 11.3 μm band with carbonates (Bregman 1977) has been confuted by McCarthy et al. (1978) and subsequently been replaced by an identification with hydrocarbons (Cohen et al. 1986), there has been continuous and recently even increased interest in carbonates as stardust and planetary dust components. Carbonate bands at wavelengths larger than 25 μm came to the fore; Erard et al. (2000) and Lellouch et al. (2000) suggested calcite and siderite ($FeCO_3$) as carriers of aerosol absorption bands of the Martian atmosphere inter alia at 26.5, 30–31, and 43.5 μm.

Kemper et al. (2002a, 2002b), by a careful analysis of the 2.4–200 μm data of the planetary nebula NGC 6302 taken with the *Infrared Space Observatory* (*ISO*), were able to show that the previously unidentified "92" μm emission band and the 62 μm component of the 60 μm emission complex in this nebula can possibly be attributed to calcite and dolomite, respectively. According to their model fit, the carbonates belong to the cold (30–60 K) dust component of this nebula.

Chiavassa et al. (2005) studied the 60–180 μm *ISO* spectra of more than 30 protostars and detected a solid state feature peaking between 90 and 110 μm in 17 of these spectra. Again, calcite has been suggested as the feature carrier, even though the accompanying characteristic resonance features of calcite could not be detected in the respective sources for different reasons (partly related to the sensitivity of the *ISO* detectors). For two star-forming regions,

[1] Based on observations with *ISO*, an ESA project with instruments funded by ESA member states (especially the PI countries: France, Germany, the Netherlands, and the United Kingdom) and with the participation of ISAS and NASA.

the Carina Nebula and Sharpless 171, this band had already been discovered by Onaka & Okada (2003) but had been ascribed to Onion structured carbon grains. The variation in the band position has been explained by Chiavassa et al. by varying amounts of other than calcium ions (e.g., Mg or Fe ions) in the carbonatic carrier.

The astronomical observations summarized so far indicate a need for more detailed investigations in two respects: (1) measurement of infrared (IR) properties below 0°C and (2) investigation of variations in the band profiles due to particle shape and size effects. Both are best achieved on the basis of determining optical constants for low temperatures. Furthermore, this approach makes it possible to get rid of the possible influence of the matrix effect which may have influenced part of the previous comparisons between laboratory and observational data on carbonates.

Given that it is unclear how carbonates can form in a circumstellar environment, Ferrarotti & Gail (2005) examined the formation of calcium carbonate in an oxygen-rich stellar wind (C/O < 1) by thermodynamic calculations, assuming the formation of calcite from Ca, H_2O, and CO. They came to the conclusion that calcite, if at all, would rather form in asymptotic giant branch (AGB) stars with *low* mass-loss rates (approximately $1 \times 10^{-6}\ M_\odot\ \mathrm{yr}^{-1}$) than in AGB stars in their superwind phase (of which planetary nebulae [PNs] like NGC 6302 are the remnants however). But also in low mass-loss–rate AGB stars, less than 1% of the total amount of dust would be carbonate dust. According to Ferrarotti & Gail (2005) it is mainly the relatively low condensation temperature of carbonates which makes their condensation in circumstellar environments so inefficient; for this temperature range to be reached in an expanding circumstellar shell, the dust must have a substantially larger distance from the central star (and, accordingly, a substantially reduced material density) than for the silicates.

Toppani et al. (2005), however, suggest a possibly (more) efficient formation mechanism of carbonates in the post-AGB phase of stellar evolution. Based on laboratory experiments, they predict carbonate formation by reactions between a comparatively hot silicate gas and a 300–500 K H_2O-CO_2–rich gas under conditions far from local thermal equilibrium (LTE). They assume this non-LTE cabonate formation to take place when high-velocity winds of forming PNs interact with dense remnants of the slow-wind AGB phase. A major goal of our study is to contribute to an assessment of the validity of the "carbonate hypotheses" from the spectroscopic point of view.

The structure of the present paper is the following. In § 2 we describe the derivation of optical constants of $CaCO_3$ and $CaMg[CO_3]_2$ from reflectance measurements, for both room and cryogenic temperatures. In § 3 absorption efficiency spectra of small calcite and dolomite grains are presented. Finally, in § 4 we compare these small-particle spectra with IR bands of astronomical objects which have been attributed to carbonates in recent studies. For the case of calcite, we present new constraints on the particle shapes and temperatures which are necessary to reconcile the 92 μm band assignments by Kemper et al. (2002a) and Chiavassa et al. (2005) with currently available laboratory data.

2. REFLECTANCE SPECTROSCOPY AND DERIVATION OF THE OPTICAL CONSTANTS

2.1. *Crystallographic Properties and Sample Preparation*

Calcite and dolomite both belong to the trigonal crystal class; hence, they are both uniaxial, and polarized reflectance measurements are required to determine their optical constants.[2] The space group of calcite is $R\bar{3}c$, while dolomite belongs to the space group $R3$ and has a reduced symmetry compared to its chemically simpler relative. While the calcium ions occupy crystallographically equivalent sites in $CaCO_3$, half of the places occupied by Ca ions in calcite are occupied by Mg ions in dolomite. The reduced symmetry of dolomite compared to calcite leads to the occurrence of an additional IR band (which is located close to 33 μm) in its spectrum. For more details on the lattice structure of Mg and Ca carbonates, see Hellwege et al. (1970) and references therein (e.g., Wyckhoff 1964).

In order to perform polarized reflectance spectroscopy, planes containing the respective crystal's *c*-axes need to be found or to be produced. This is a difficult task in the case of ordinary $CaCO_3$ or $CaMg[CO_3]_2$ rhombohedra, since none of their surfaces fulfill this condition. The *c*-axis runs diagonally through the obtuse corners of cleaved rhombohedra.

In the case of our dolomite rhombohedron, a $2 \times 2 \times 2$ cm^3 crystal from Eugui, Navarra (Spain), it was therefore necessary to cut it in order to produce a *c*-parallel surface, which has been subsequently polished. Polarized reflectance measurements on the polished surfaces showed no "mixing" of the ordinary and extraordinary ray, which proved the cut to be parallel to the *c*-axis indeed. In the case of our calcite crystal (a $4 \times 2 \times 1$ cm^3 fragment of a prisma found in Sweetwater, MO) no cut was necessary, because this individual crystal had a relatively rare stature, its long edges having grown parallel to the symmetry axis. Hence, polishing one of the lateral surfaces of this crystal was sufficient to obtain a large measuring spot containing the *c*-axis. Indeed, polarized spectroscopy on that spot did not show significant traces of mixing of the two principal orientations of the electric field vector relative to *c* ($E \parallel c$, $E \perp c$; see also Fig. 1).

2.2. *Reflectance Spectroscopy*

The reflectance spectra of our two samples have been measured at near-normal incidence using a Fourier transform infrared (FTIR) spectrometer Bruker 113v in the wavelength range 2–120 μm at a resolution of 2 cm^{-1}. Gold mirrors have been used as references. A turnable grid polarizer on polyethylene substrate positioned at the entrance of the sample compartment was used to select polarization directions parallel and normal to the plane of incidence.

Figure 1 shows reflectance spectra of calcite in the 5–120 μm range, which comprises all IR bands of this mineral. In the case of the reflectance for the ordinary ray ($E \perp c$), an offset of 1.0 has been added to all reflectance values. The different line styles correspond to the different temperatures (10–300 K) as indicated.

For the ordinary ray, five reflection bands can be discerned in the IR spectrum of calcite, which are centered at 6.8, 14.0, 30.7, 44.0, and 91.4 μm for room temperature. For the extraordinary ray, the respective reflectance band positions amount to 11.4, 29.6, and 91.4 μm (again for room temperature).

In Figure 2 the reflectance spectra of dolomite are plotted on the same scale as for calcite. Dolomite has a slightly more complex band pattern than calcite, which is a consequence of its comparatively reduced lattice symmetry mentioned in § 2.1. The reflectance maxima are located at 6.6, 13.8, 25.5, 38.4, and 61.7 μm for the ordinary ray (at $T = 300$ K), while for the extraordinary ray, the respective positions are 11.3, 25.4, 31.6, 56.7, and 60.0 μm.

For the cryogenic measurements, the experimental setup was the following: the samples have been placed into a continuous-flow liquid-helium cryostat with contact-gas cooling (CryoVac KONTI Spectro B) equipped with polyethylene windows. It was inserted into the FTIR spectrometer's sample compartment at the same position where the room-temperature reflection measurements

[2] Interestingly, the phenomenon of *birefringence* has been first observed in calcite crystals.

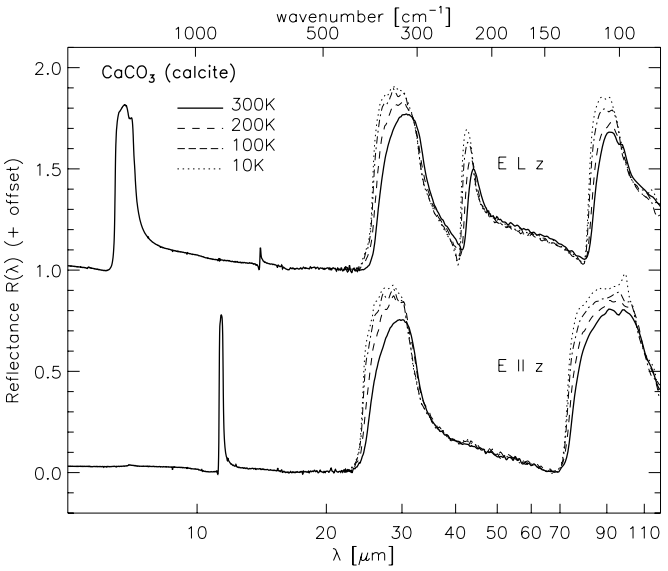

FIG. 1.—Polarized reflectance spectra of calcite for $T = 300$ K (*solid line*), 200 K (*dashed line*), 100 K (*dash-dotted line*), and 10 K (*dotted line*). The spectra for $E \perp c$ were shifted vertically by an amount of 1.0.

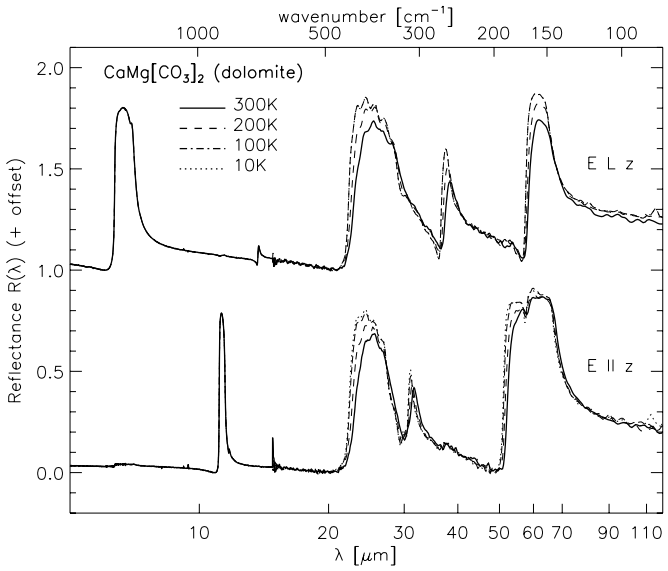

FIG. 2.—Same as Fig. 1, but for dolomite.

had been performed. The cryostat windows did not allow measurements at wavelengths shorter than 15 μm. The cryostat possesses two sample mounts which can alternatingly be moved into the IR beam, thus allowing subsequent measurements on the sample and the reference mirror at each temperature. A third measurement with the sample tilted to suppress the reflection was necessary (again at each temperature) in order to determine the reflectivity of the cryostat windows ("zero signal"), which had to be subtracted from both the sample and reference spectra. The temperature was controlled by means of a CryoVac temperature controller using an ohmic heater and two silicon diode temperature sensors connected to the liquid-helium–cooled walls of the contact gas chamber and to the sample mount. The temperatures have been stable to about ± 0.5 K during the measurements.

Spectra have been taken at 200, 100, and 10 K during cooling down the samples. Two cooling cycles have been carried out for each sample with the two polarizer orientations. The wavelength- and temperature-dependent reflectances have been calculated by dividing the "zero-corrected" sample and reference spectra at each temperature.

It is found that for both dolomite and calcite, all bands in the above indicated wavelength range undergo a shift to shorter wavelengths, a bandwidth decrease, and band strength increase with decreasing temperatures. These effects are especially significant for calcite's 44 μm reflectance band and for dolomite's 38 μm reflectance band. A more detailed discussion is given in § 3.

2.3. *Lorentz Oscillator Fits and Derived Optical Constants*

The polarized reflectance spectra of calcite and dolomite can be quite accurately reproduced by Lorentz oscillator fits, as has been shown, e.g., by Hellwege et al. (1970). Using the *Ansatz*

$$\epsilon(\nu) = \epsilon_\infty + \sum_j \frac{\Omega_j^2}{\mathrm{TO}_j^2 - \nu^2 - i\gamma_j \nu}, \qquad (1)$$

where ϵ_∞ is the dielectric constant for frequencies that are large compared to all IR wavelengths and Ω_j, TO_j, and γ_j are the strength, transverse optical phonon frequency, and damping constant of the jth oscillator, respectively.

Figure 3 shows the optical constants of calcite which have been derived from the polarized reflectance spectra by means of Lorentz oscillator fits. The oscillator parameters which were used for these fits, five oscillators for the ordinary ray and three for the extraordinary ray, are listed in Table 1.

For dolomite, we only list its oscillator parameters, six oscillators for the ordinary ray and five for the extraordinary ray (see Table 2), while the optical constants are not shown. However, both for calcite and dolomite, the optical constants can be retrieved from the AIU Jena Database of Optical Constants for Cosmic Dust,[3] which also includes graphs.

Apart from the different number of oscillators, another important difference between calcite's and dolomite's IR spectra is the absence of any phonon band for the latter at wavelengths larger than 67 μm (or wavenumbers smaller than 150 cm^{-1}). In other words, it is noteworthy that calcite's IR bands extend to wavelengths roughly 1.5 times larger than dolomite's "reddest" band.

For 300 K, our oscillator parameters are quite comparable with those derived by Hellwege et al. (1970), except for some minor bands which are missing in their measurements (e.g., our "4_{ER}" for dolomite), probably due to a spectral resolution that is somewhat too small.

3. SMALL-PARTICLE SPECTRA FOR DIFFERENT SHAPE DISTRIBUTIONS

From the optical constants shown and discussed in § 2.3, the absorption cross sections per particle volume, C_{abs}/V, have been calculated for grains of different shapes. Since the focus of this paper is on bands at large wavelengths, we choose the limit of particles being small compared to the wavelength (Rayleigh limit, size parameter $x = 2\pi a/\lambda \ll 1$, and $|\epsilon^{1/2}|x \ll 1$, with a being the grain radius or largest semidiameter).

The following grain shapes have been taken into account: spheres (according to the Mie theory) and continuous distributions of ellipsoids (CDEs). As for the latter, two different modifications of it have been used: a CDE with equal probability for all ellipsoid axis ratios ("mean CDE"; after Bohren & Huffman 1983) and a

[3] See the Web site at http://www.astro.uni-jena.de/Laboratory/OCDB.

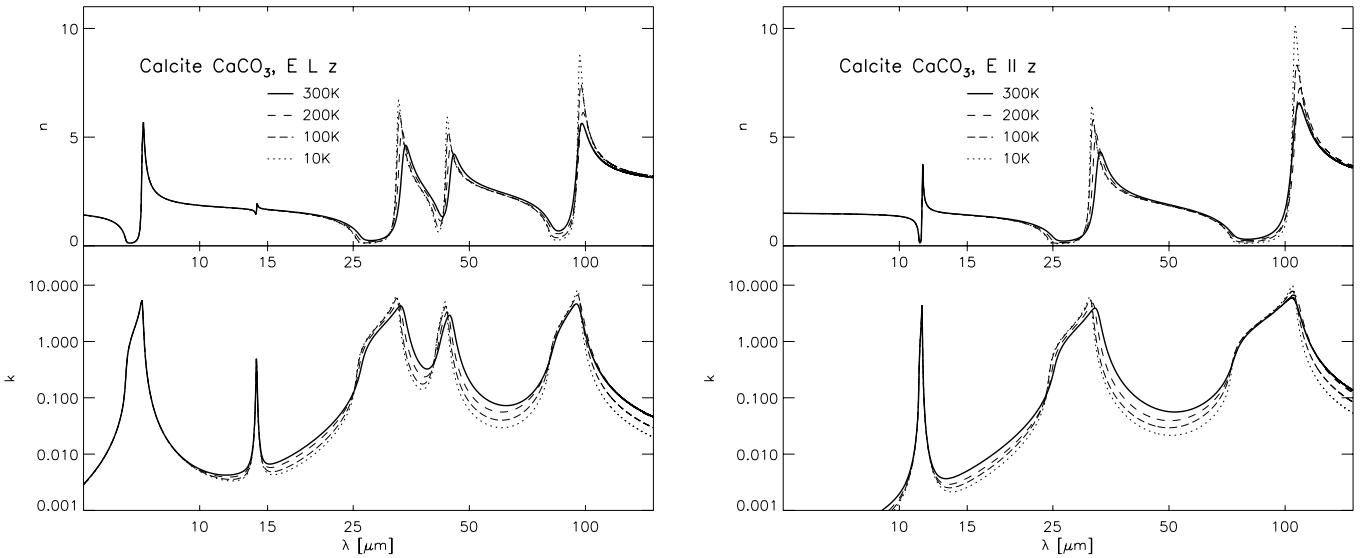

FIG. 3.—Optical constants of calcite for room temperature, 200, 100, and 10 K for the ordinary ray ($E \perp c$; *left*) and for the extraordinary ray ($E \parallel c$; *right*).

CDE with maximum probability for spherical grains ("weighted CDE"; after Ossenkopf et al. 1992).

3.1. *Temperature Effects for Spherical Grains*

Figures 4 and 5 show the volume-normalized absorption cross sections C_{abs}/V calculated for spherical calcite and dolomite grains, respectively, depending on temperature. The figures demonstrate that the effect of the cooling on the band positions and bandwidths is also present in the small-particle spectra. Like the reflectance

TABLE 1

LORENTZ OSCILLATOR PARAMETERS DERIVED FOR CALCITE

j	TO_j (cm^{-1})	Ω_j (cm^{-1})	γ_j (cm^{-1})
1_{OR}	1407.4	1039.6	14.8
2_{OR}	712.0	71.4	4.0
$3_{OR,300K}$	297.0	377.7	15.7
$3_{OR,200K}$	302.5	385.4	12.0
$3_{OR,100K}$	306.0	387.0	8.87
$3_{OR,10K}$	307.1	387.6	7.34
$4_{OR,300K}$	222.8	206.1	11.0
$4_{OR,200K}$	226.5	211.2	8.35
$4_{OR,100K}$	228.8	219.1	6.14
$4_{OR,10K}$	229.7	219.7	4.54
$5_{OR,300K}$	104.7	148.1	6.00
$5_{OR,200K}$	103.2	165.7	5.35
$5_{OR,100K}$	103.8	158.0	3.57
$5_{OR,10K}$	104.2	167.6	2.45
1_{ER}	872.0	250.8	2.09
$2_{ER,300K}$	306.7	368.0	16.9
$2_{ER,200K}$	312.6	372.2	11.6
$2_{ER,100K}$	317.6	377.6	9.19
$2_{ER,10K}$	318.9	378.7	7.30
$3_{ER,300K}$	94.3	200.6	7.10
$3_{ER,200K}$	93.3	203.2	5.91
$3_{ER,100K}$	94.6	203.6	4.37
$3_{ER,10K}$	95.0	202.4	2.86

NOTES.—"OR" refers to the ordinary ray and "ER" refers to the extraordinary ray. Where no temperature is indicated as subscript, oscillator parameters have been derived from room-temperature measurements. For the dielectric background, we chose the value $\epsilon_{inf,OR} = 2.6$ in the case of OR and $\epsilon_{inf,ER} = 2.3$ in the case of ER.

TABLE 2

SET OF LORENTZ OSCILLATOR PARAMETERS DERIVED FOR DOLOMITE BY FITTING THE ROOM-TEMPERATURE REFLECTANCE SPECTRA

j	TO_j (cm^{-1})	Ω_j (cm^{-1})	γ_j (cm^{-1})
1_{OR}	1453.8	399.2	23.8
2_{OR}	1425.5	980.0	15.0
3_{OR}	727.3	98.8	6.14
$4_{OR,300K}$	348.7	459.0	22.1
$4_{OR,200K}$	351.5	462.5	16.0
$4_{OR,100K}$	356.0	464.4	12.0
$4_{OR,10K}$	355.9	464.5	11.9
$5_{OR,300K}$	259.1	190.6	9.86
$5_{OR,200K}$	261.1	201.9	7.97
$5_{OR,100K}$	263.4	201.5	5.58
$5_{OR,10K}$	263.4	201.4	5.54
$6_{OR,300K}$	152.9	209.1	5.18
$6_{OR,200K}$	152.9	214.2	3.42
$6_{OR,100K}$	153.5	214.9	2.26
$6_{OR,10K}$	153.5	214.7	2.20
1_{ER}	874.9	301.0	2.98
$2_{ER,300K}$	364.8	335.8	20.4
$2_{ER,200K}$	368.5	341.8	16.3
$2_{ER,100K}$	370.7	349.8	12.7
$2_{ER,10K}$	371.5	356.4	11.9
$3_{ER,300K}$	316.8	179.5	9.13
$3_{ER,200K}$	319.4	175.6	8.24
$3_{ER,100K}$	321.3	168.1	6.05
$3_{ER,10K}$	321.6	178.0	5.05
$4_{ER,300K}$	171.9	30.5	8.76
$4_{ER,200K}$	174.0	29.2	6.42
$4_{ER,100K}$	174.4	31.1	5.56
$4_{ER,10K}$	174.8	34.4	4.97
$5_{ER,300K}$	150.3	243.2	3.35
$5_{ER,200K}$	151.2	247.5	3.29
$5_{ER,100K}$	151.4	249.8	2.31
$5_{ER,10K}$	152.2	260.4	2.17

NOTE.—All designations have the same meaning as in the previous table, but here we chose $\epsilon_{inf,OR} = 2.7$ and $\epsilon_{inf,ER} = 2.4$.

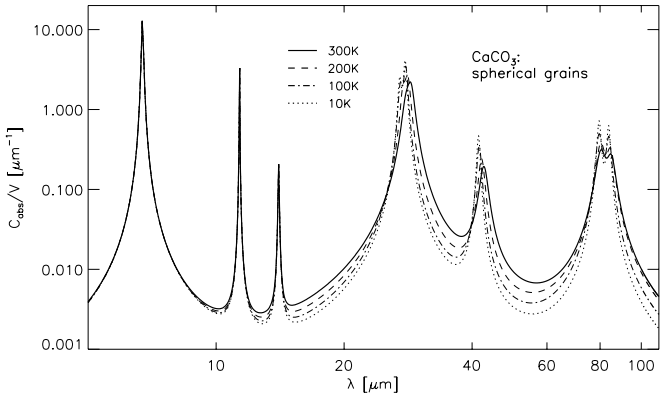

FIG. 4.—Volume normalized absorption cross sections of spherical calcite grains for room temperature, 200, 100, and 10 K in the wavelength range 5–110 μm.

spectra, this effect is especially pronounced for the case of the $\sim$40 μm band of calcite, which shifts from 42.6 μm for 300 K to 41.4 μm for 10 K, while at the same time, the C_{abs}/V peak value increases by a factor of 2.4. For the calcite bands around 30 and 80 μm, the temperature dependence is not equally strong, but still significant.

In the case of $CaMg[CO_3]_2$, the temperature-dependent evolution of the spectra is similar apart from the effect that there is only an insignificant change between 100 and 10 K (see Fig. 5). For the additional band in the dolomite spectrum (compared to calcite) around 31 μm, the temperature dependence is rather moderate compared to the other bands. In the wavelength range $\lambda < 15$ μm, the dolomite and the calcite spectra resemble each other very closely.

3.2. *Grain-Shape Effects at Low Temperatures*

Because of the high oscillator strengths characterizing most of the IR bands of both calcite and dolomite, the grain-shape dependence of the band profiles is very strong. For the far-IR (FIR) bands of calcite, this is evident from the comparison of Figure 4 with Figure 6, as well as from the peak wavelengths given in Table 3. Calcite's 30 μm band is shifted to the "red" by about 2 μm for a mean CDE compared to the case of spherical grains, and at the same time its width is increased by factor of 4. The 80–90 μm double band of calcite degenerates into a broad single bump centered at 90.1 μm with two wings for the mean CDE. For the weighted CDE case, the maximum of the absorption efficiency is located at 86.3 μm for a grain temperature of 300 K. For the 40 μm band, the broadening due to the shape distribution is not equally strong as for the 80–90 μm band, and the shift of the band position to longer wavelengths is limited to 1 μm for a given temperature (compared to more than 5 μm for the 80–90 μm band).

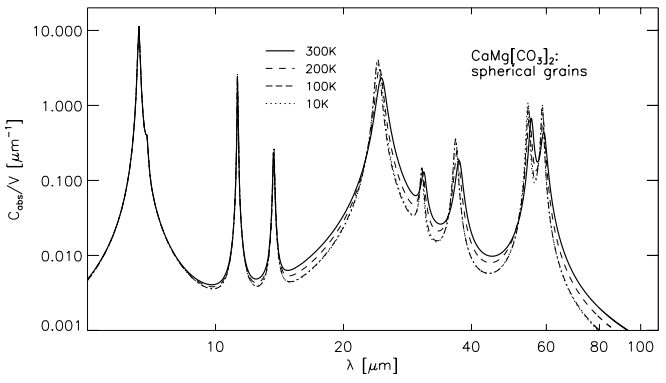

FIG. 5.—Same as Fig. 4, but for dolomite.

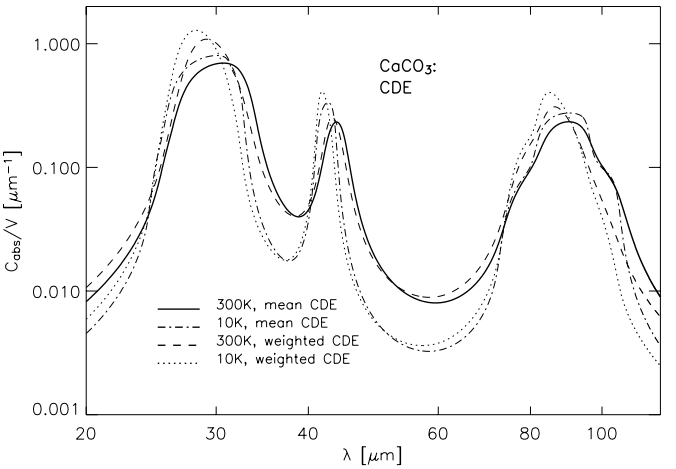

FIG. 6.—The C_{abs}/V profiles for a distribution of ellipsoidally shaped calcite grains (see text for details). Only the wavelength range 20–120 μm and only the two temperature "extremes" $T = 10$ and 300 K have been depicted here.

Comparing the band properties for different temperatures within a given grain model, we find that the shift of the peak position is still very prominent in the case of the 40 μm feature for the grain-shape distributions. It clearly dominates over shape effects for this band, whereas this is not true for the 30 and 80–90 μm features. In the case of the latter, both the shape effects are stronger due to the higher oscillator strengths, and the temperature effects are intrinsically smaller, as discussed in § 3.1.

3.3. *Comparison to PE Powder Spectra*

Since powder spectra of calcite and dolomite, measured at room temperature, have been used by both Kemper et al. (2002a) and Chiavassa et al. (2005) in order to argue for the presence of carbonate dust in astronomical objects, it is important to discuss the relation between such powder spectra and the small-particle spectra based on our optical constants. By "powder spectra" or "PE spectra," we mean the transmission spectra of submicron-sized ground powder embedded in polyethylene (PE), transformed into absorption cross sections. Powder spectra generally depend on various circumstances such as particle size and shape, orientation, agglomeration degree, and the refractive index of the surrounding medium (e.g., Bohren & Huffman 1983).

TABLE 3

POSITIONS OF THE MAXIMA OF C_{abs}/V FOR CALCITE GRAINS AT DIFFERENT TEMPERATURES AND FOR DIFFERENT SHAPE DISTRIBUTIONS

Peak Position	20 μm Complex (μm)	40 μm (μm)	80–90 μm (μm)
Sphere			
10 K	27.05, 27.84	41.40	79.62, 83.77
300 K	28.58	42.64	80.56, 84.71
Weighted CDE			
10 K	28.18	41.75	84.91
300 K	29.13	43.09	86.25
Mean CDE			
10 K	30.02	42.54	90.31
300 K	30.66	43.68	90.14

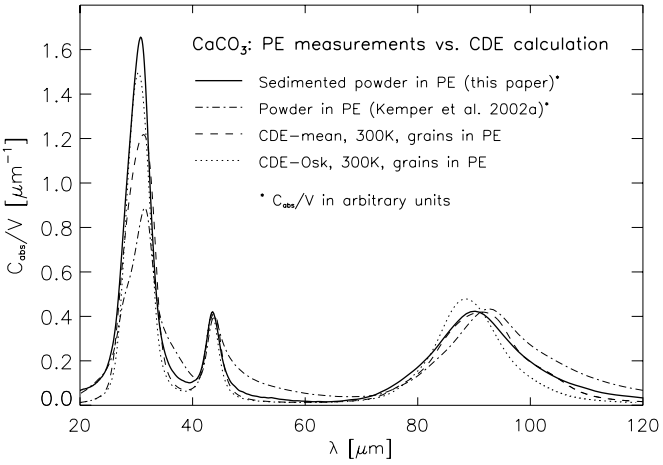

FIG. 7.—Comparison of calcite's FIR bands measured by PE powder transmission spectroscopy (*solid and dashed-dotted lines*; see text for details) with the absorption efficiency spectrum calculated from the optical constants for a mean continuous distribution of ellipsoids (*dashed lines*) and for a weighted CDE (*dotted lines*), both in PE.

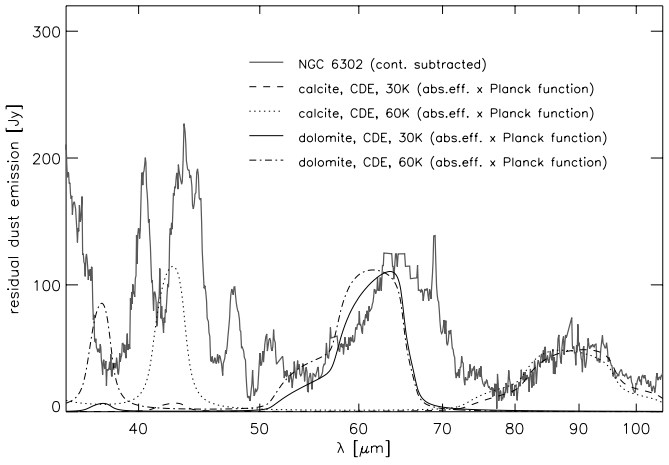

FIG. 8.—Comparison between the residual dust emission of NGC 6302 and synthetic dust emission spectra (for 30 and 60 K) of calcite and dolomite in the 35–105 μm range.

Figure 7 shows both the powder spectrum published by Kemper et al. (2002a), measured on a sample of unsedimented calcite grains (*dash-dotted line*), and of a sample of calcite grains which had previously been subjected to sedimentation in a liquid (acetone), in order to remove large grains (*solid line*). The peak of the latter spectrum is shifted by about 2 μm to shorter wavelengths with respect to the data published by Kemper et al. (2002a), although both have been measured at room temperature. This is due to the presence of large grains (several microns in diameter) in the unsedimented powder. The spectrum of the sedimented powder is in good agreement with the result of the calculation for a *mean* CDE with a PE environment (see Fig. 7), indicating the presence of a considerable fraction of grains with shapes far away from spherical symmetry.

Conversely, we find that the mean CDE is a good representation of the shape distribution of a real calcite powder with grain sizes within the Rayleigh limit. This justifies the use of this shape distribution for the comparison with observed data at large wavelengths. In § 4.1 we apply this model to simulate dust spectra at low temperatures.

4. COMPARISON WITH ASTRONOMICAL OBSERVATIONS

The laboratory spectra presented so far are especially relevant for a comparison with FIR spectra of cold dust in objects such as the PN NGC 6302. Hence, we shall first give a brief review of some key properties of the dust spectrum of this object.

Barlow (1997) observed features at 65 and 69 μm and another possible broadband feature in the range of 88–98 μm. While the 65 μm feature was attributed to crystalline ice (see also Waters et al. 1996), the 69 μm feature was suspected to be due to crystalline forsterite, and the question of the carrier of the 88–98 μm band remained open.

Molster et al. (2001) identified the ~65 μm band as a blend of diopside and crystalline water ice with enstatite. They also confirmed the reality of the broad feature around 90 μm and suspected that there should be a very cold dust component present in the nebula.

Kemper et al. (2002a, 2002b) first assigned the ~65 μm feature to cold dolomite (with additional contributions by diopside and water ice) and the broad emission band around 90 μm to cold calcite dust. As already mentioned above, the temperature of the carbonate dust was assumed to be in the 30–60 K range. A mass fraction of less than 0.3% (for calcite as well as for dolomite) has been derived by these authors. We retrieved an *ISO* Short Wavelength Spectrometer (SWS) and an *ISO* Long Wavelength Spectrometer (LWS) spectrum of NGC 6302 from the *ISO* archive and reduced it by means of OLP version 10.0.

From the composite spectrum (ranging from 2.4 to 200 μm), we subtracted a combination of Planck functions for temperatures of 30, 55, and 95 K. The remaining "residual dust emission" is shown in Figure 8 for the 35–105 μm range; the individual broad peaks of the gray line result from various ice and dust species such as H_2O, forsterite, enstatite, diopside, and possibly carbonates (see Table 2 in Kemper et al. 2002a).

Our aim has been to examine whether the assignments of the 60–65 μm and 92 μm bands to dolomite and calcite are compatible with the optical constants and powder spectra presented in § 3, and if so, for which temperatures and particle shapes this is the case. In answering these questions, the detectability of bands at wavelengths between 35 and 45 μm depending on the dust temperature also plays a key role.

4.1. *The* 92 μm *Band in NGC 6302*

A detailed view of the 92 μm band is given in Figure 9. It can be seen from this figure (when compared to Fig. 6) that only for a mean CDE particle shape distribution of calcite grains, the bandwidth is as large as in the case of the NGC 6302 spectrum. For a weighted CDE, the bandwidth is smaller by 45% (at the relevant cryogenic temperatures). The best fit is achieved by the $C_{\rm abs}/V$ function for a mean CDE multiplied by a Planck function for a temperature of 30 K. A dust temperature of 60 K is hardly compatible with the observations, both with respect to the 92 μm band profile and with respect to the emergence of a ~42 μm feature (see dotted lines in Figs. 8 and 9). The calcite data derived from transmission spectroscopy of *sedimented* powder (Fig. 9, *dash-dotted line*) roughly reproduce the observed band profile as well. It is noteworthy that the 92 μm band profile of NGC 6302 obtained by Kemper et al. (2002a) is better fitted by the PE spectrum of an *unsedimented* calcite powder sample which is broader and peaks at a larger wavelength. This may be due to the use of different *ISO* LWS spectra (a mean of seven spectra vs. a single spectrum) or due to some uncertainty in the continuum subtraction.

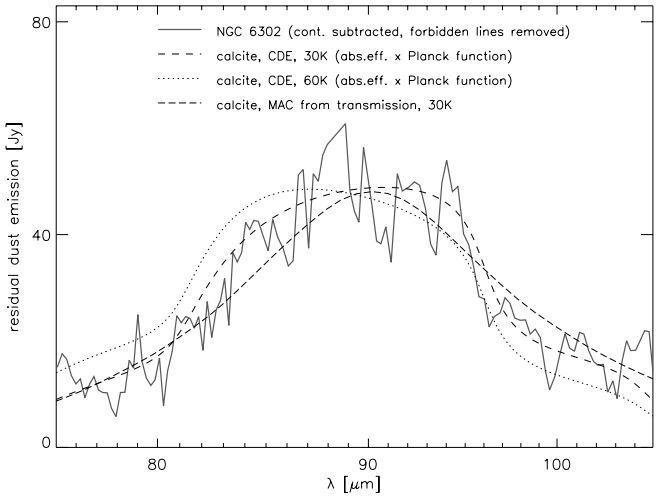

FIG. 9.—Comparison between the residual dust emission of NGC 6302 and synthetic dust emission spectra of ensembles of ellipsoidally shaped calcite grains for 30 and 60 K in the 75–105 μm range.

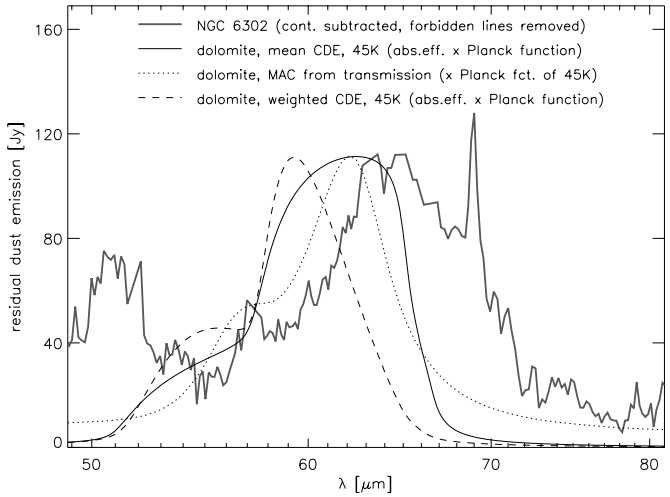

FIG. 10.—Comparison between the residual dust emission of NGC 6302 and synthetic dust emission spectra of ensembles of ellipsoidally shaped dolomite grains for 30 and 50 K in the 49–81 μm range.

4.2. *The* 60–65 μm *Emission Complex in NGC 6302*

In Figure 10 a close-up view of the 60 μm emission complex is shown. Although the bandwidth of a mean CDE particle-shape distribution can reproduce the observed bandwidth of the 60 μm feature, neither for a mean CDE nor for a weighted CDE, both at a temperature of 45 K, do the *positions* coincide with that observed. The difference between the band positions resulting from laboratory measurements and the observed band position ($\sim$64 μm) is too large as to be compensated by temperature effects (see also Fig. 8, where a comparison with dolomite dust at $T = 30$ K is made). Dust temperatures lower than 40 K would allow the suppression of the dolomite emission band at $\sim$37 μm (see again Fig. 8), but the position of the 60 μm feature would still not match. Therefore, this feature cannot be fit only by dolomite, while dolomite's contribution to the "blue wing" of the 60 μm emission complex is not excluded. Our study confirms that the 60–65 μm band must have other major carriers, e.g., diopside, as suggested by Kemper et al. (2002a), or saponite, as suggested by Hofmeister & Bowey (2006). A recent publication by Chihara et al. (2007) shows that a mixture of diopside and åkermanite ($Ca_2MgSi_2O_7$) at a temperature of 30 K provides a good match of the 60–65 μm feature.

4.3. *The* 90–110 μm *Band in Protostars*

Chiavassa et al. (2005) studied a sample of 32 low- and intermediate-mass protostars (mostly Class 0 and Herbig Ae/Be objects). Out of this sample, 17 sources show a broadband feature between 90 and 110 μm. The dust temperature in these objects is found by blackbody fits to the continuum to be below 50 K (except for emission from the innermost regions). Calcite is suggested to be a possible carrier of this feature, which seems to be supported by the laboratory measurements of Kemper et al. (2002a) that show a peak at 93 μm and a width (FWHM) of 16 μm.

Our data show that for PE powder measurements on small grains and also for calculated spectra assuming a mean CDE, the maximum of the 92 μm calcite band is located at 90 μm. For other particle-shape distributions, it is narrower and located at much smaller wavelengths, especially for the temperature range relevant for PNs and protostars. The transverse optical resonance wavelength of mode $5_{OR,10K}$ of about 96 μm (Table 1) can be considered as the maximum peak position for this band (see Bohren & Huffman 1983). The feature produced by the $3_{ER,10K}$ mode with a TO resonance wavelength of about 105 μm is much broader and, therefore, comparably weak and cannot dominate the calcite grain emission even if alignment effects were present.

Hence, we conclude that the bands observed for the Herbig Ae/Be objects may in principle be compatible with emission from calcite grains, if sufficiently extreme shape distributions (much more extreme than the mean CDE) and/or large grains are assumed (cf. Fig. 7 in Chiavassa et al. 2005). For the Class 0 objects, on the contrary, we confirm that the feature characteristics are incompatible with laboratory data for calcite. Whether the incorporation of other ions into a carbonate can shift the band to still larger wavelengths must be left open at this point.

5. CONCLUSIONS

While previous studies on carbonate dust in astronomical environments were largely based on powder measurements performed at room temperature, we have on the one hand derived optical constants of calcite and dolomite and on the other hand carried out measurements at cryogenic temperatures (200, 100, and 10 K). From these optical constants, small-particle spectra (absorption efficiencies as functions of the wavelength and temperature) were calculated for different grain shapes.

Since the optical constants of calcite and dolomite reach peak values of 5–10 (corresponding to maxima of the imaginary part of the dielectric function of up to 150), their absorption efficiencies are extremely sensitive to particle-shape effects. For example, for the 92 μm band of calcite, the negativity range of the real part of the dielectric function is as large as 73–96 μm for the ordinary ray (and even 75–105 μm for the extraordinary ray). The former values approximately indicate how large the range is in which calcite's 92 μm band can shift due to particle-shape effects, since the ordinary ray is weighted more strongly than the extraordinary ray.

At cryogenic temperatures, the FIR bands of calcite and dolomite increase their intensity, get narrower, and shift to shorter wavelengths. The temperature-related shift in position is largest for calcite's 40 μm band; in this case, it reaches 0.5 μm per 100 K.

As for the 92 μm feature detected by Kemper et al. (2002a) in *ISO* LWS spectra of NGC 6302, this feature can only be assigned to $CaCO_3$ grains if the assumption of a mean CDE, with equal probability of all grain shapes, is made.

Furthermore, dust temperatures have to be well below 40 K in order to suppress the 30 μm and 42 μm bands of calcite which accompany the 92 μm band but are not seen in the spectra of NGC 6302.

We thank Gabriele Born and Walter Teuschel (Jena) for sample preparation and help with the cryogenic measurements. Ingrid Hodouš kindly provided the *ISO* spectrum of NGC 6302, reduced with the *ISO* spectral analysis package ISAP. H. M. acknowledges support by Deutsche Forschungsgemeinschaft (DFG) grant Mu 1164/5. T. P. acknowledges support by the DFG Forschergruppe laboratory astrophysics, by a grant from the Max Planck Society. A. B. has been supported by the Austrian Fonds zur Förderung der wissenschaftlichen Forschung (FWF; project P18939-N16). Comments by an anonymous referee helped to improve the original version of this paper.

REFERENCES

Barlow, M. J. 1997, Ap&SS, 255, 315
Bohren, C. F., & Huffman, D. R. 1983, Absorption and Scattering of Light by Small Particles (New York: Wiley)
Bregman, J. D. 1977, PASP, 89, 335
Bregman, J. D., & Rank, D. M. 1975, ApJ, 195, L125
Chiavassa, A., Ceccarelli, C., Tielens, A. G. G. M., Caux, E., & Maret, S. 2005, A&A, 432, 547
Chihara, H., Koike, C., & Tsuchiyama, A. 2007, A&A, 464, 229
Cohen, M., et al. 1986, ApJ, 302, 737
Erard, S., Lellouch, E., Encrenaz, T., Morris, P., de Graauw, T., & Burgdorf, M. 2000, LPI, 31, 1325
Ferrarotti, A. S., & Gail, H.-P. 2005, A&A, 430, 959
Gillett, F. C., Forrest, W. J., & Merrill, K. M. 1973, ApJ, 183, 87
Hellwege, K. H., Lesch, W., Plihal, M., & Schaack, G. 1970, Z. Physik, 232, 61
Hofmeister, A. M., & Bowey, J. E., 2006, MNRAS, 367, 577
Joswiak, D. J., & Brownlee, D. E. 2001, LPI, 32, 1998
Kemper, F., Molster, F. J., Jäger, C., & Waters, L. B. F. M. 2002a, A&A, 394, 679
Kemper, F., et al. 2002b, Nature, 415, 295
Lellouch, E., et al. 2000, Planet. Space Sci., 48, 1393
Lisse, C. M., VanCleve, J., & Adams, A. C. 2006, Science, 313, 635
McCarthy, J. F., Forrest, W. J., & Houck, J. R. 1978, ApJ, 224, 109
Molster, F. J., et al. 2001, A&A, 372, 165
Onaka, T., & Okada, Y. 2003, ApJ, 585, 872
Ossenkopf, V., Henning, Th., Mathis, J. S. 1992, A&A, 261, 567
Penman, J. M. 1976, MNRAS, 176, 539
Quirico, E., et al. 2000, LPI, 31, 1260
Sandford, S. A. 1986, Science, 231, 1540
Tomeoka, K., & Buseck, P. R. 1986, Science, 231, 1544
Toppani, A., et al. 2005, Nature, 437, 1121
Waters, L. B. F. M., et al. 1996, A&A, 315, L361
Wyckhoff, R. W. G. 1964, Crystal Structures, Vol. 2 (2nd ed.; New York: Sydney Interscience)